NANO LETTERS

pubs.acs.org/NanoLett

Letter

Inorganically Connecting Colloidal Nanocrystals Significantly Improves Mechanical Properties

Zhongyong Wang, Soundarya Srinivasan, Rui Dai, Ashish Rana, Qiong Nian, Kiran Solanki, and Robert Y. Wang*

Cite This: *Nano Lett.* 2023, 23, 4916−4922

Read Online

ACCESS | Metrics & More | Article Recommendations | Supporting Information

ABSTRACT: Understanding and characterizing the mechanical behavior of colloidal nanocrystal (NC) assemblies are important for developing nanocrystalline materials with exceptional mechanical properties for robust electronic, thermoelectric, photovoltaic, and optoelectronic devices. However, the limited ranges of Young's modulus, hardness, and fracture toughness ($\lesssim$1−10 GPa, $\lesssim$50−500 MPa, and $\lesssim$10−50 kPa $m^{1/2}$, respectively) in as-synthesized NC assemblies present challenges for their mechanical stability and therefore their practical applications. In this work, we demonstrate using a combination of nanoindentation measurements and coarse-grained modeling that the mechanical response of assemblies of as-synthesized NCs is governed by the van der Waals interactions of the organic surface ligands. More importantly, we report tremendous ∼60× enhancements in Young's modulus and hardness and an ∼80× enhancement in fracture toughness of CdSe NC assemblies through a simple inorganic $Sn_2S_6^{4-}$ ligand exchange process. Moreover, our observation of softening in nanocrystalline materials with decreasing CdSe NC diameter is consistent with atomistic simulations.

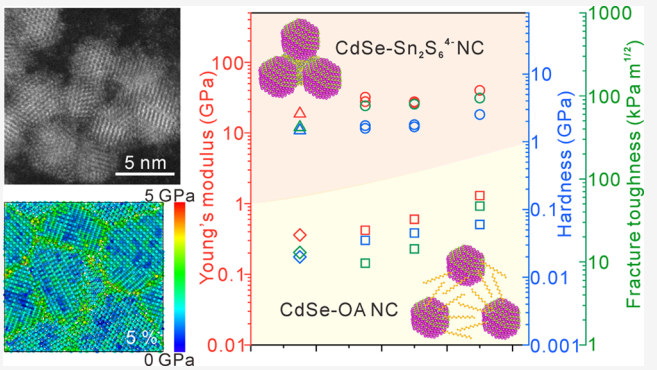

KEYWORDS: *nanocrystal, inorganic ligands, mechanical properties, coarse-grained model, atomistic molecular dynamics*

The mechanical behavior of nanocrystalline materials, which are characterized by numerous grain boundaries, has been extensively studied over the past ∼25 years due to their superior properties compared to conventional polycrystalline materials.[1−6] Using electrodeposition,[7] inert gas condensation,[8] mechanical alloying/milling,[9] crystallization from amorphous alloys,[10] and intense plastic deformation,[11] researchers have synthesized nanocrystalline materials that surpass conventional polycrystalline materials in terms of fracture toughness,[12] strength and hardness,[1] and mechanical/thermal stability.[2] Despite their efficacy, these techniques often present challenges in controlling interface structure, grain size distribution, and impurity levels within the nanocrystalline materials. Consequently, a comprehensive understanding of mechanical properties in nanocrystalline materials and the ability to design them pose significant hurdles.

Colloidal nanocrystals (NCs) have well-controlled sizes and shapes, faceted boundaries, and surface chemistry,[13,14] making them an intriguing platform for mechanical property studies on nanocrystalline materials. The mechanical characteristics of colloidal NCs are also of practical importance, as these materials are being considered for applications such as photovoltaics,[15−18] thermoelectrics,[18−20] transistors,[18,21] and optoelectronics.[18,22] Successfully implementing colloidal NCs in these applications will require appropriate mechanical properties alongside their more studied electrical, optical, and thermal properties. Comprehension and manipulation of NC assembly mechanical properties are consequently both critical and underinvestigated.

The mechanical properties of as-synthesized colloidal NCs are generally poor and fall within a narrow range of $\lesssim$1−10 GPa and $\lesssim$50−500 MPa for Young's modulus and hardness, respectively.[23] More recent measurements[24,25] indicate a fracture toughness of ∼50 kPa $m^{1/2}$ for organic ligand capped NC assemblies, reflecting their brittle nature. Researchers have developed several approaches to improve the mechanical robustness of colloidal NC assemblies, including ligand removal,[26] ligand cross-linking,[27,28] organic ligand exchange,[29] and NC ordering.[30,31] Nevertheless, these techniques are either limited to certain types of NC systems or only result in marginal improvements.

In this work, we report up to 60× enhancements in both Young's modulus and hardness and an 80× enhancement in

Received: February 20, 2023
Revised: May 22, 2023
Published: May 31, 2023

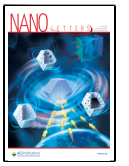

https://doi.org/10.1021/acs.nanolett.3c00674
Nano Lett. 2023, 23, 4916−4922

fracture toughness for CdSe NC assemblies that have had their organic ligands between adjacent NCs replaced with a thin tin disulfide layer. We create this thin tin disulfide layer through the utilization of inorganic metal chalcogenide complex (MCC) ligands that were originally developed to improve charge transport in NC assemblies.[32] In a recent study,[33] it was discovered that MCC ligands undergo spontaneous dissociation, forming an amorphous passivation layer that acts as a bridge between adjacent NCs. We use nanoindentation to measure the Young's modulus, hardness, and fracture toughness. To gain insights into our data, we utilize a combination of coarse-grained modeling, atomistic molecular dynamics, and density functional theory simulations. These integrated experimental measurements and computational models indicate that the replacement of the organic ligands with inorganic tin disulfide leads to covalent NC−NC interfaces that significantly improves mechanical properties.

We synthesized monodisperse CdSe NCs with diameters ranging from 3.5 to 7.0 nm and CdS magic-sized clusters (MSCs, diameter ∼1.5 nm) with organic oleic acid (OA) ligands and inorganic $Sn_2S_6^{4-}$ ligands using modified literature recipes.[32,34−36] We characterized the NCs using a range of imaging techniques, including transmission electron microscopy (TEM), scanning transmission electron microscopy (STEM), and scanning electron microscopy (SEM). TEM (Figure 1a and Figure S1) and high-magnification high-angle annular dark-field (HAADF) STEM images (Figure 1g) indicated a space between neighboring NC cores, which is attributed to the presence of an organic ligand shell encompassing the NC surface. As schematically illustrated in Figure 1b and demonstrated in the literature,[37,38] these OA ligands are believed to partially interdigitate due to ligand−ligand attractions. On the other hand, CdSe-$Sn_2S_6^{4-}$ NCs have very small interparticle spacings, as shown in the HAADF STEM images (Figure 1d,h) and schematically illustrated in Figure 1e (where interparticle spacing denotes the distance from the edge of one NC core to the edge of the adjacent NC core). This very small interparticle spacing is a result of the ligand exchange with the much smaller $Sn_2S_6^{4-}$ ligand, and the subsequent/spontaneous room-temperature dissociation of $Sn_2S_6^{4-}$ into amorphous tin disulfide.[33] Notably, in the case of inorganic ligands, CdSe NCs are bridged by a thin SnS_x layer, but not sintered, as high-resolution HAADF STEM images show no sign of lattice merging of neighboring NCs (Figure 1h and Figure S5a). This is further supported by the invariant grain size determined from XRD (Figure S8) and similar excitonic peaks from UV/vis spectra (Figure S6) of organic and inorganic ligand capped CdSe NC films. Additional UV−vis spectra (Figure S2) show that CdS-OA MSCs possess an excitonic absorption peak of 410 nm, which allows us to specify an effective diameter of ∼1.5 nm for the MSC as based on empirical sizing curves of CdS NCs.[39] As a comparison, 3.5 and 7 nm CdSe-OA NCs show excitonic absorption peaks of ∼534 and ∼655 nm, respectively (Figures S2 and S6).

Smooth films were successfully prepared by drop-casting and subsequently drying concentrated solutions of NC and MSC. Cross-sectional SEM images of OA (Figure 1c)- and $Sn_2S_6^{4-}$ (Figure 1f)-capped 3.5 nm CdSe NC films demonstrate that these films have a thickness of ∼3 μm. Local elemental mapping (Figure S5) on inorganic ligand capped 7 nm CdSe NC films reveals a coating of tin and sulfur on the CdSe NC cores. We also collected larger area EDS spectra of both types

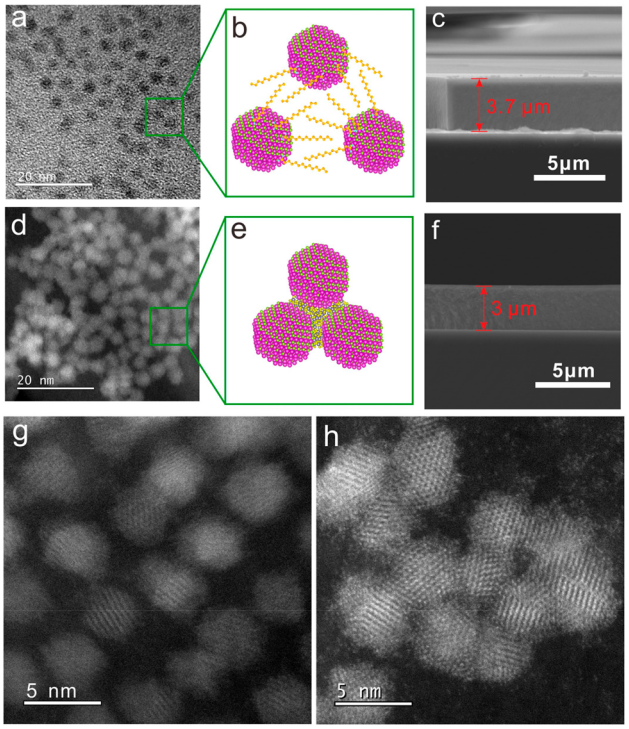

Figure 1. Characterizations of CdSe nanocrystals (NCs) with oleic acid (OA) ligands and $Sn_2S_6^{4-}$ ligands; (a) TEM image showing a submonolayer of 3.5 nm NCs with OA ligands; (b) schematic depiction of interdigitated organic ligands on adjacent NCs; (c) cross-sectional SEM image of a sample film consisting of OA-capped NCs; (d) low-resolution HAADF STEM image showing a submonolayer of 3.5 nm $Sn_2S_6^{4-}$-capped NCs; (e) schematic representation of 3.5 nm NCs that are bridged by a few atomic layers of amorphous SnS_2; (f) cross-sectional SEM image of a sample film consisting of $Sn_2S_6^{4-}$-capped NCs; high-resolution HAADF STEM images displaying submonolayers of (g) 3.5 nm OA-capped NCs and (h) 3.5 nm $Sn_2S_6^{4-}$-capped NCs.

of CdSe NC films (Figure S4a,b), which indicate the presence of OA and SnS_x on the CdSe NC surface for organic and inorganic ligand capped CdSe NC films, respectively. An additional EDS analysis of inorganic ligand films without NCs (Figure S4c) exhibits a Sn:S atomic ratio of ∼1:2.4. This is further complemented by inductively coupled plasma mass spectroscopy (ICP-MS, Table S6), which indicates that the Sn:S atomic ratio is 1:2 for our CdSe NCs with inorganic ligands. The ICP-MS data also show that our CdSe NCs are metal-rich and the concentrations of amorphous SnS_2 are generally low and inversely proportional to CdSe NC diameters. The low concentration of SnS_2 is also evidenced by XRD (Figure S8) and TGA (Figure S7), which do not show SnS_2 XRD peaks and undergo only a ∼ 6% mass loss when heated to 350° C.

Our analysis of the nanoindentation results suggests that the Young's modulus and hardness of NC and MSC assemblies can be significantly enhanced by a factor of up to 60 by exchanging the original OA ligands with inorganic $Sn_2S_6^{4-}$ ligands. Specifically, the schematics in Figure 2a,b illustrate the nanoindentation behavior of CdSe-OA and CdSe-$Sn_2S_6^{4-}$ NC assemblies, respectively. Representative load−displacement curves and SEM images of clean indents on the CdSe-OA and CdSe-$Sn_2S_6^{4-}$ NC assemblies are shown in Figure 2c,d, respectively. Consistent with previous measurements on

https://doi.org/10.1021/acs.nanolett.3c00674
Nano Lett. 2023, 23, 4916−4922

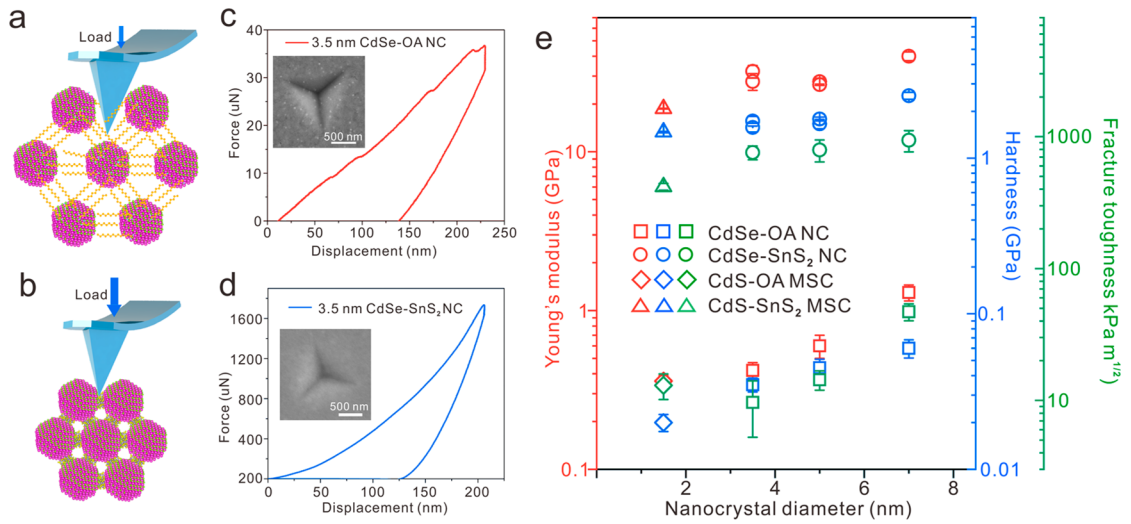

Figure 2. Nanoindentation results on CdSe-OA NC and CdSe-$Sn_2S_6^{4-}$ NC thin films. Schematic illustrations of behaviors of (a) CdSe-OA NC thin films and (b) CdSe-$Sn_2S_6^{4-}$ NC thin films during the nanoindentation tests (to better illustrate the difference in mechanical response, the nanoindentation tips are not drawn to scale). Representative force−displacement curves of (c) OA-capped NC thin films and (d) $Sn_2S_6^{4-}$-capped NC thin films, respectively. The insets of (c) and (d) show the SEM images of representative indents for OA-capped NC and $Sn_2S_6^{4-}$-capped NC thin films, respectively. (e) Comparison of Young's modulus, hardness, and fracture toughness of CdSe NC and CdS MSC assemblies that are functionalized with OA ligands and $Sn_2S_6^{4-}$ ligands, respectively.

analogous materials,[30] our data (Figure 2e) confirm that OA-capped NC assemblies with diameters ranging from 3.5 to 7.0 nm exhibit a narrow range of Young's modulus (0.3−1.3 GPa) and hardness (20−60 MPa). In contrast, CdSe-$Sn_2S_6^{4-}$ NC assemblies of various core sizes (3.5−7.0 nm) exhibit a much larger Young's modulus (18−38 GPa) and hardness (1.5−2.5 GPa). Both OA- and $Sn_2S_6^{4}$-capped NC assemblies exhibit an increased Young's modulus and hardness as the NC diameter increases. This trend of increasing Young's modulus and hardness with NC diameter has been previously observed for organically capped NCs.[31,40] Our previous work[31] indicates that the size dependence of mechanical properties in OA-capped NC assemblies originates from varied ligand−ligand interactions as the NC diameter changes. In the case of $Sn_2S_6^{4-}$-capped NC assemblies, we hypothesize that grain boundary activity accounts for the size dependence in Young's modulus and hardness. We note that our samples did exhibit microscale film cracking; however, the distance (∼100 μm) between cracks is much larger than the nanoindent size (∼1 μm). Consequently, our measurements should not be impacted by these cracks (Figure S3).

Nanoindentation experimental data when combined with energy analysis[41] allow us to derive the fracture toughness of the CdSe NC assemblies (Figure 2e and Section IIb of the Supporting Information). Specifically, we find that CdSe-OA NC assemblies exhibit fracture toughnesses of ∼10−47 kPa $m^{1/2}$, which is in the same magnitude as previous measurements[25] on 7 nm PbS-OA NC superlattices. These low fracture toughnesses reveal the brittle nature of NC assemblies with organic ligands. The extremely low fracture toughness originates from the weak intermolecular forces between the adjacent organic ligands as well as poor ligand interdigitation that lowers the energy dissipation before fracture. On the other hand, after inorganic ligand functionalization, the fracture toughness of CdSe-$Sn_2S_6^{4-}$ NC assemblies increase to ∼420−940 kPa $m^{1/2}$ (up to ∼80× enhancement greater than CdSe-OA NC assemblies). This tremendous improvement is largely due to replacing the van der Waals interactions of organic ligands with covalent interfacial bonds that significantly increase the energy dissipation before material failure.

To further understand the size dependence of Young's modulus and hardness, we employ the coarse-grained model developed in our previous work[31] to simulate the mechanical properties of organic ligand capped NC assemblies. As schematically demonstrated in Figure 3a, an NC pair includes two neighboring NCs and two ligand shells that overlap as a result of partial ligand interdigitation. The interparticle attraction between adjacent NCs in the CdSe-OA system arises from three primary contributors: the ligand−ligand van der Waals (vdW) interactions, dipole−dipole interactions between the cores, and the core−core vdW interactions. Figure S9 demonstrates that the ligand−ligand interaction surpasses both the core−core vdW interaction and the dipole−dipole interaction, highlighting the dominant influence of ligand−ligand vdW attraction on the mechanical response of the CdSe-OA system.

We then created face-centered-cubic (FCC) NC periodic assemblies of different diameters with their corresponding pairwise potentials (Figure 3a). This assumption of FCC packing for OA-capped CdSe NCs is reasonable, as FCC is the most frequently observed packing structure for OA-capped NCs.[30,42] The mechanical properties of the constructed NC assembly were determined by its stress−strain relation, as detailed in Section III of the Supporting Information. Specifically, as illustrated in Figure 3b, we applied tensile strain to the NC assembly along the ⟨100⟩ direction until structure failure. Representative stress−strain curves are shown in Figure 3c.

The effectiveness of our coarse-grained model is demonstrated in Figure 3d,e, where the experimental data align well with the model in both magnitude and trend. Through our combined measurements and modeling, we establish the ligand−ligand interaction as the principal factor governing the mechanical strength of OA-capped NC assemblies. This conclusion agrees with previous molecular dynamics simulations.[43] We also evaluate the bulk modulus, shear modulus,

https://doi.org/10.1021/acs.nanolett.3c00674
Nano Lett. 2023, 23, 4916−4922

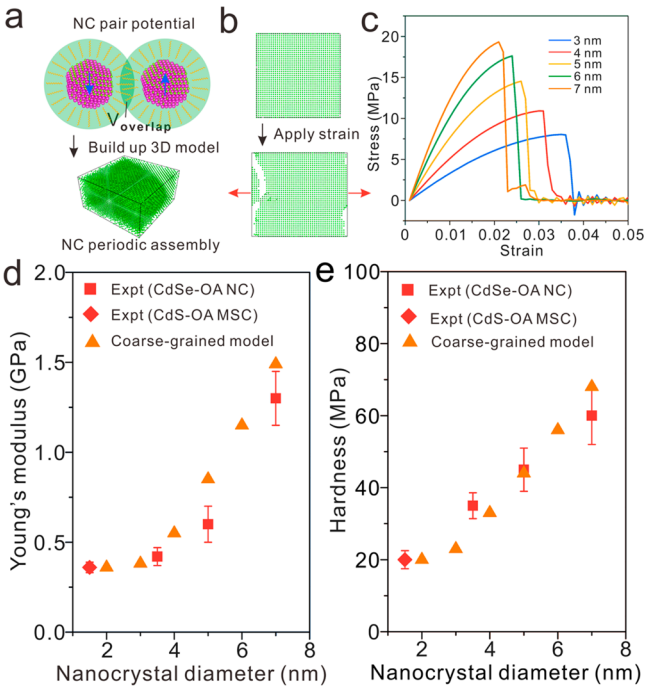

Figure 3. Analysis of Young's modulus and hardness of OA-capped NC assemblies determined with coarse-grained modeling that is based upon a NC pair potential. (a) Top: illustration of two interacting CdSe NCs, consisting of a NC core and an organic ligand shell. The ligand shells partially overlap within a volume denoted as $V_{overlap}$; the CdSe NC cores possess permanent dipoles (blue arrows shown on NC cores) attributed to the spontaneous polarization of the CdSe wurtzite lattice. Bottom: construction of a three-dimensional face-centered-cubic (FCC) model using the NC pair potential. (b) Application of tensile stress along the ⟨100⟩ lattice direction of the FCC model, with the corresponding strain recorded to generate the stress−strain curves illustrated in (c). (d) Dependence of Young's modulus on the NC core diameter (3.5−7.0 nm), including results obtained from our coarse-grained model (triangles). The red diamonds correspond to OA-capped CdS MSC assemblies. (e) Variation of hardness of NC film assemblies in relation to NC diameter along with simulated results from our coarse-grained model. The red diamonds in (e) correspond to OA-capped CdS MSC assemblies.

yield strength, and Poisson ratio of OA-capped NC assemblies using the coarse-grained model, as shown in Table S1. We computed toughness by integrating stress−strain curves (Table S2). The exceptionally low yield strength (i.e., 7.9 MPa for 3.5 nm OA-capped CdSe NC) and toughness (i.e., 0.18 MJ/m^3 for 3.5 nm OA-capped CdSe NC) demonstrate the brittle nature of these CdSe-OA NC assemblies. According to classical mechanics theory,[44] the hardness of a material can be calculated as $Y \times N$, where Y represents yield strength and N is a fitting constant. We determine that N is ∼2.5 based upon a satisfactory fit to our experimental measurements (Figure 3e). Previous works[44,45] have derived a N value of 2 for polymers. It is not surprising that organically capped NC assemblies exhibit behavior similar to polymers, as their mechanical properties largely depend on molecular ligand interactions.

Unlike organically capped CdSe NC assemblies, tin disulfide bridged CdSe NC assemblies possess significantly enhanced mechanical properties (Figure 2e). Specifically, our measured Young's modulus of 40 GPa for inorganic ligand capped 7 nm CdSe NCs is consistent with the bulk Young's modulus of wurtzite CdSe (40.4 GPa).[46] Inorganically capped CdSe NC films of smaller core sizes (<7 nm) exhibit a reduced modulus, which can be potentially attributed to grain boundaries and/or nanoporosity. Additional calculations performed in Section IIIc of the Supporting Information reveal that the interaction energies resulting from vdW and electrostatic interactions between the NC cores are considerably smaller than the dissociation energy of covalent bonds. This finding strongly suggests that the primary source of mechanical enhancement in $Sn_2S_6^{4-}$-capped NC assemblies originates from the covalent nature of the chemical bonds formed within the system.

Next, we studied nanocrystalline CdSe using atomistic molecular dynamics (MD) simulations (Section IV of the Supporting Information) as a proxy for understanding our data on CdSe-$Sn_2S_6^{4-}$ NC assemblies. We do not explicitly include the Sn−S interfacial layer in our model due to a lack of appropriate potentials for describing covalent interactions among Cd, Se, Sn, and S. In addition, the interfacial Sn−S phase is ultrathin and not clearly distinguishable from the CdSe boundaries (Figure 1h). Hence, while not ideal, a simplified MD model describing nanocrystalline CdSe is potentially insightful. We created nanocrystalline CdSe of average grain size ranging from 1.2 to 7.2 nm. Unlike the FCC packing used in our organically capped NC simulations, the nanograins in these simulations are randomly packed. Figure 4a shows a representative snap short of 6 nm nanocrystalline CdSe. The model is then subjected to strain until failure to derive stress−strain curves (Figure 4c).

The Young's modulus derived from the stress−strain curves increases with larger grain sizes, which agrees with experiments (Figure 4d). However, there is an offset between these two sets of results, which could be due to neglect of interfacial S and Sn atoms and/or neglect of defects (e.g., nanovoids) in the model. We tried different strain rates (10^9/s and 10^8/s) in our MD simulations, and this had only a minor effect on the stress−strain curves (Figure S13). Further, we determined the yield strength of nanocrystalline CdSe from the stress−strain curves. Nanocrystalline CdSe shows a softening with smaller grain sizes in our atomistic MD simulations (Figure S14). The derived yield strength was further converted into hardness through the classical relationship $H = Y \times N$. The converted hardness matches with experimental results (Figure 4e) with an N value of 0.8. Such a small N might be ascribed to the presence of nanoporosity as in earlier work,[44,45] which indicated an N value of 1 for porous materials. The simulated von Mises stress distributions at various strains, as depicted in Figure 4b and Figure S15, reveals the presence of stress concentration at grain boundaries, which indicates that grain boundary activity (i.e., grain sliding) governs the plastic deformation. This phenomenon elucidates the observed softening of nanocrystalline CdSe with reduced grain sizes, as grain boundary activity facilitates plastic deformation processes. Moreover, the observation of crack opening in all nanocrystalline CdSe models, as shown in Figure S15, signifies that intergranular fracture is the dominant fracture mode. Lastly, we compute the toughness, which is defined by the area under the stress−strain curve and listed in Table S4. The toughness of nanocrystalline CdSe increased significantly once the organic ligands were removed. This tremendous increase is a result of increased energy dissipation from the grain boundary activity when nanocrystalline CdSe is plastically deformed.

https://doi.org/10.1021/acs.nanolett.3c00674
Nano Lett. 2023, 23, 4916−4922

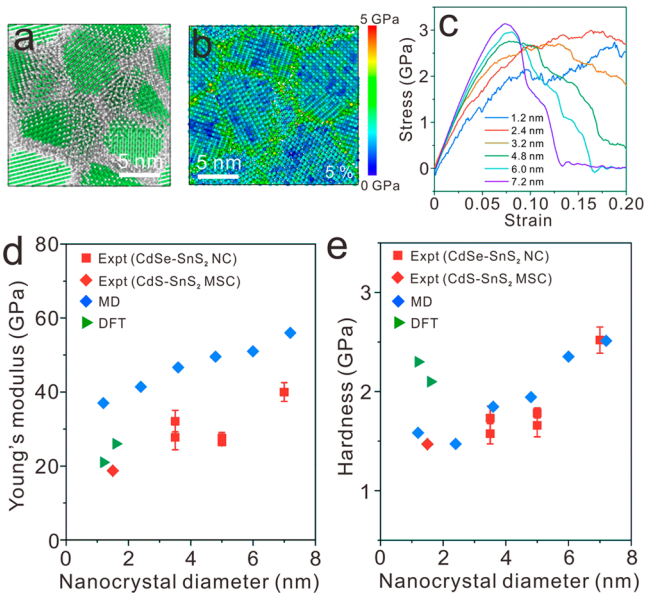

Figure 4. Atomistic modeling of nanocrystalline CdSe based on molecular dynamics and density functional theory, along with their experimental comparison. (a) Visualization of a 6 nm nanocrystalline CdSe material generated through atomistic molecular dynamics simulation. The interior Cd and Se atoms are denoted in green, while the Cd and Se atoms at the boundary are indicated in gray. (b) von Mises stress distribution within the 6 nm nanocrystalline CdSe shown in (a) under a tensile strain of 5%, which reveals a stress concentration at the boundaries. (c) Stress–strain plots of nanocrystalline CdSe with varying grain sizes subjected to a tensile strain at a rate of 10^9/s. (d) Young's modulus and (e) hardness of CdSe-$Sn_2S_6^{4-}$ NC and MSC thin film assemblies as a function of NC diameter. The diamonds shown in (d) and (e) are CdS MSC with $Sn_2S_6^{4-}$ ligands.

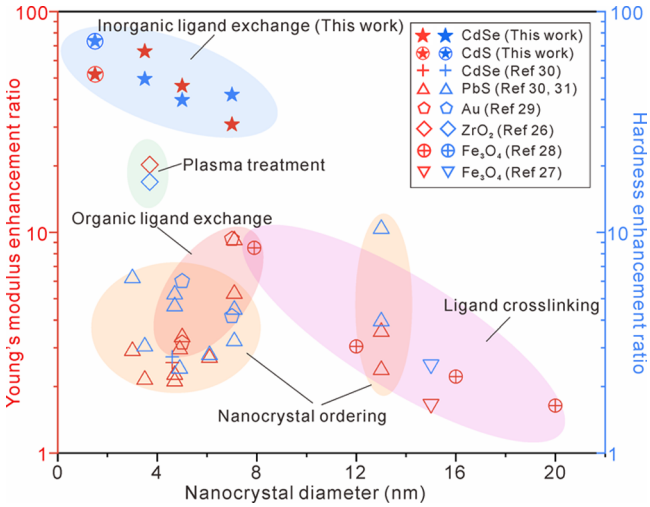

Figure 5. Comparison of Young's moduli and hardness enhancement ratios for this work (inorganic ligand exchange) relative to those of other approaches in the literature.

We further utilized density functional theory (DFT) simulations to understand how the interfacial bonds are related to the mechanical properties of CdSe-SnS_2 NC assemblies (Section V of the Supporting Information and Figure S16).[47] As shown in Figure 4d, the DFT simulation results and experimental results for Young's modulus of CdS MSC-SnS_2 are in reasonable agreement (21 and 19 GPa, respectively). Additional DFT simulations suggest that bulk amorphous SnS_2 and a CdSe wurtzite lattice exhibit Young's moduli of 63 and 41 GPa, respectively. This indicates that the CdSe/SnS_2 interface is the mechanical weak point. We did not attempt DFT simulations on larger NC core diameters due to their extremely high computational cost.

Our DFT results can be combined with the analytical model proposed by Gao et al.[48] to derive the hardness of the CdSe/SnS_2 structure (Section VI of the Supporting Information). As indicated in Figure 4e, the DFT model yields the right order of magnitude but overestimates hardness by ~50%. This variance could be potentially attributed to omission of plastic deformation mechanisms (such as bending and rotation) beyond the bond breaking described in Gao's model. Additionally, DFT simulations reveal that adjusting the core size and ligand composition also leads to changes in the Young's modulus and hardness of SnS_x-capped CdSe NCs, as shown in Figure S17. Other important mechanical properties are also calculated and listed in Table S5.

Finally, to compare this inorganic ligand exchange approach with other literature approaches, we summarize enhancement ratios for Young's modulus and hardness in Figure 5. We define the enhancement ratio as the post-treatment property divided by the original property of the as-synthesized NCs with organic ligands (a version of Figure 5 that uses absolute values is available as Figure S18 in the Supporting Information). It can be seen that the inorganic ligand exchange approach exhibits significantly larger enhancement ratios than that achieved with plasma treatment,[26] organic ligand exchange,[29] ligand cross-linking,[27,28] and NC ordering.[30,31] Moreover, the inorganic MCC ligand exchange can be applied to a variety of semiconductor and noble-metal NCs, which presents a greater potential for mechanically robust devices based upon semiconductor NCs and noble-metal NCs.

In summary, we reported more than 60-fold enhancements of Young's modulus, hardness, and fracture toughness of colloidal NCs with inorganic functionalization. We first demonstrated that the presence of weak ligand–ligand vdW interactions within organically capped NC assemblies leads to poor mechanical properties. We then verified this using a coarse-grained model. We further showed that inorganically connected NC assemblies feature strong covalent interactions and thereby lead to large mechanical reinforcement. It is important to highlight that inorganic functionalization represents a versatile method to enhance the mechanical properties of colloidal NCs. Unlike alternative methods involving etching or annealing, inorganic functionalization offers distinct advantages, particularly for semiconductor NCs and noble-metal NCs. We further performed atomistic simulations upon inorganically capped NC assemblies to understand the role of boundaries in determining their mechanical properties. We expect that our study will stimulate further research in the mechanical properties of colloidal NC systems employing alternative inorganic chemistry.[49−51] The colloidal chemistry approach demonstrated in this study enables the preparation of nanocrystalline materials with precise control over their shape, size, and interfaces, thereby offering immense potential for fundamental studies and the exploration of distinctive mechanical properties. The development of robust nanocrystalline thin films through solution processing holds great promise for various mechanical coating applications.[52]

https://doi.org/10.1021/acs.nanolett.3c00674
Nano Lett. 2023, 23, 4916−4922

■ ASSOCIATED CONTENT

Supporting Information

The Supporting Information is available free of charge at https://pubs.acs.org/doi/10.1021/acs.nanolett.3c00674.

Detailed descriptions, figures, and data on materials synthesis and characterization (TEM, SEM, optical images, UV−vis spectra, ICP-MS, EDS, TGA, XRD), mechanical measurements and analysis, fracture toughness analysis, pair potential and coarse-grained modeling, atomistic molecular dynamics simulations, density functional theory simulations, and intrinsic hardness simulations, as well as additional figures and tables (PDF)

■ AUTHOR INFORMATION

Corresponding Author

Robert Y. Wang − *School for Engineering of Matter, Transport & Energy, Arizona State University, Tempe, Arizona 85281, United States;* orcid.org/0000-0002-3888-6906; Email: rywang@asu.edu

Authors

Zhongyong Wang − *School for Engineering of Matter, Transport & Energy, Arizona State University, Tempe, Arizona 85281, United States;* Present Address: Department of Mechanical Engineering, University of Michigan, Ann Arbor, Michigan 48109, United States

Soundarya Srinivasan − *School for Engineering of Matter, Transport & Energy, Arizona State University, Tempe, Arizona 85281, United States*

Rui Dai − *School for Engineering of Matter, Transport & Energy, Arizona State University, Tempe, Arizona 85281, United States*

Ashish Rana − *School for Engineering of Matter, Transport & Energy, Arizona State University, Tempe, Arizona 85281, United States*

Qiong Nian − *School for Engineering of Matter, Transport & Energy, Arizona State University, Tempe, Arizona 85281, United States*

Kiran Solanki − *School for Engineering of Matter, Transport & Energy, Arizona State University, Tempe, Arizona 85281, United States;* orcid.org/0000-0002-4385-620X

Complete contact information is available at: https://pubs.acs.org/10.1021/acs.nanolett.3c00674

Author Contributions

Z.W. and R.Y.W. proposed and conceived the study. Z.W. synthesized, fabricated, and characterized the samples. A.R. assisted with sample characterization. S.S. performed the nanoindentation experiments under the supervision of K.S. R.D. performed molecular dynamics simulation under the supervision of Q.N.. Z.W. performed density functional theory simulations and additional modeling. The manuscript was jointly written by all authors with the main contributions from Z.W. and R.Y.W. All authors have given approval for the final version of the manuscript.

Notes

The authors declare no competing financial interest.

■ ACKNOWLEDGMENTS

This work was supported by the National Science Foundation CAREER program through award number DMR-1654337. We gratefully acknowledge the use of facilities within the Eyring Materials Center at Arizona State University.

■ REFERENCES

(1) Bringa, E. M.; Caro, A.; Wang, Y. M.; Victoria, M.; McNaney, J. M.; Remington, B. A.; Smith, R. F.; Torralva, B. R.; Van Swygenhoven, H. Ultrahigh Strength in Nanocrystalline Materials under Shock Loading. *Science* **2005**, *309*, 1838−1841.

(2) Li, X. Y.; Jin, Z. H.; Zhou, X.; Lu, K. Constrained Minimal-Interface Structures in Polycrystalline Copper with Extremely Fine Grains. *Science* **2020**, *370*, 831−836.

(3) Schiotz, J.; Di Tolla, F. D.; Jacobsen, K. W. Softening of Nanocrystalline Metals at Very Small Grain Sizes. *Nature* **1998**, *391*, 561−563.

(4) Lu, L.; Sui, M. L.; Lu, K. Superplastic Extensibility of Nanocrystalline Copper at Room Temperature. *Science* **2000**, *287*, 1463−1466.

(5) Meyers, M. A.; Mishra, A.; Benson, D. J. Mechanical Properties of Nanocrystalline Materials. *Prog. Mater. Sci.* **2006**, *51*, 427−556.

(6) Madhav Reddy, K.; Guo, J. J.; Shinoda, Y.; Fujita, T.; Hirata, A.; Singh, J. P.; McCauley, J. W.; Chen, M. W. Enhanced Mechanical Properties of Nanocrystalline Boron Carbide by Nanoporosity and Interface Phases. *Nat. Commun.* **2012**, *3*, 1052.

(7) Erb, U. Electrodeposited Nanocrystals: Synthesis, Properties and Industrial Applications. *Nanostruct. Mater.* **1995**, *6*, 533−538.

(8) Nieman, G. W.; Weertman, J. R.; Siegel, R. W. Microhardness of Nanocrystalline Palladium and Copper Produced by Inert-Gas Condensation. *Scripta Metall. Mater.* **1989**, *23*, 2013−2018.

(9) Suryanarayana, C. Mechanical Alloying and Milling. *Prog. Mater. Sci.* **2001**, *46*, 1−184.

(10) Lu, K.; Wang, J. T.; Wei, W. D. A New Method for Synthesizing Nanocrystalline Alloys. *J. Appl. Phys.* **1991**, *69*, 522−524.

(11) Iwahashi, Y.; Wang, J. T.; Horita, Z.; Nemoto, M.; Langdon, T. G. Principle of Equal-Channel Angular Pressing for the Processing of Ultra-Fine Grained Materials. *Scripta Mater.* **1996**, *35*, 143−146.

(12) Qin, E. W.; Lu, L.; Tao, N. R.; Tan, J.; Lu, K. Enhanced Fracture Toughness and Strength in Bulk Nanocrystalline Cu with Nanoscale Twin Bundles. *Acta Mater.* **2009**, *57*, 6215−6225.

(13) Yin, Y.; Alivisatos, A. P. Colloidal Nanocrystal Synthesis and the Organic−Inorganic Interface. *Nature* **2005**, *437*, 664−670.

(14) Boles, M. A.; Ling, D.; Hyeon, T.; Talapin, D. V. The Surface Science of Nanocrystals. *Nat. Mater.* **2016**, *15*, 141−153.

(15) Steinhagen, C.; Panthani, M. G.; Akhavan, V.; Goodfellow, B.; Koo, B.; Korgel, B. A. Synthesis of Cu_2ZnSnS_4 Nanocrystals for Use in Low-Cost Photovoltaics. *J. Am. Chem. Soc.* **2009**, *131*, 12554−12555.

(16) Ma, W.; Luther, J. M.; Zheng, H. M.; Wu, Y.; Alivisatos, A. P. Photovoltaic Devices Employing Ternary PbS_xSe_{1-x} Nanocrystals. *Nano Lett.* **2009**, *9*, 1699−1703.

(17) McDonald, S. A.; Konstantatos, G.; Zhang, S. G.; Cyr, P. W.; Klem, E. J. D.; Levina, L.; Sargent, E. H. Solution-Processed PbS Quantum Dot Infrared Photodetectors and Photovoltaics. *Nat. Mater.* **2005**, *4*, 138−142.

(18) Kagan, C. R.; Lifshitz, E.; Sargent, E. H.; Talapin, D. V. Building Devices from Colloidal Quantum Dots. *Science* **2016**, *353*, aac5523.

(19) See, K. C.; Feser, J. P.; Chen, C. E.; Majumdar, A.; Urban, J. J.; Segalman, R. A. Water-Processable Polymer-Nanocrystal Hybrids for Thermoelectrics. *Nano Lett.* **2010**, *10*, 4664−4667.

(20) Wang, R. Y.; Feser, J. P.; Lee, J. S.; Talapin, D. V.; Segalman, R.; Majumdar, A. Enhanced Thermopower in PbSe Nanocrystal Quantum Dot Superlattices. *Nano Lett.* **2008**, *8*, 2283−2288.

(21) Talapin, D. V.; Murray, C. B. PbSe Nanocrystal Solids for N- and P-Channel Thin Film Field-Effect Transistors. *Science* **2005**, *310*, 86−89.

(22) Talapin, D. V.; Lee, J. S.; Kovalenko, M. V.; Shevchenko, E. V. Prospects of Colloidal Nanocrystals for Electronic and Optoelectronic Applications. *Chem. Rev.* **2010**, *110*, 389−458.
(23) Begley, M. R.; Gianola, D. S.; Ray, T. R. Bridging Functional Nanocomposites to Robust Macroscale Devices. *Science* **2019**, *364*, eaav4299.
(24) Choi, J.; Hui, C. M.; Pietrasik, J.; Dong, H. C.; Matyjaszewski, K.; Bockstaller, M. R. Toughening Fragile Matter: Mechanical Properties of Particle Solids Assembled from Polymer-Grafted Hybrid Particles Synthesized by ATRP. *Soft Matter* **2012**, *8*, 4072−4082.
(25) Tam, E.; Podsiadlo, P.; Shevchenko, E.; Ogletree, D. F.; Delplancke-Ogletree, M. P.; Ashby, P. D. Mechanical Properties of Face-Centered Cubic Supercrystals of Nanocrystals. *Nano Lett.* **2010**, *10*, 2363−2367.
(26) Shaw, S.; Colaux, J. L.; Hay, J. L.; Peiris, F. C.; Cademartiri, L. Building Materials from Colloidal Nanocrystal Arrays: Evolution of Structure, Composition, and Mechanical Properties Upon the Removal of Ligands by O_2 Plasma. *Adv. Mater.* **2016**, *28*, 8900−8905.
(27) Dreyer, A.; Feld, A.; Kornowski, A.; Yilmaz, E. D.; Noei, H.; Meyer, A.; Krekeler, T.; Jiao, C. G.; Stierle, A.; Abetz, V.; Weller, H.; Schneider, G. A. Organically Linked Iron Oxide Nanoparticle Supercrystals with Exceptional Isotropic Mechanical Properties. *Nat. Mater.* **2016**, *15*, 522−528.
(28) Wang, Z. Y.; Singaravelu, A. S. S.; Dai, R.; Nian, Q.; Chawla, N.; Wang, R. Y. Ligand Crosslinking Boosts Thermal Transport in Colloidal Nanocrystal Solids. *Angew. Chem., Int. Ed.* **2020**, *59*, 9556−9563.
(29) Gauvin, M.; Wan, Y.; Arfaoui, I.; Pileni, M.-P. Mechanical Properties of Au Supracrystals Tuned by Flexible Ligand Interactions. *J. Phys. Chem. C* **2014**, *118*, 5005−5012.
(30) Podsiadlo, P.; Krylova, G.; Lee, B.; Critchley, K.; Gosztola, D. J.; Talapin, D. V.; Ashby, P. D.; Shevchenko, E. V. The Role of Order, Nanocrystal Size, and Capping Ligands in the Collective Mechanical Response of Three-Dimensional Nanocrystal Solids. *J. Am. Chem. Soc.* **2010**, *132*, 8953−8960.
(31) Wang, Z.; Christodoulides, A. D.; Dai, L.; Zhou, Y.; Dai, R.; Xu, Y.; Nian, Q.; Wang, J.; Malen, J. A.; Wang, R. Y. Nanocrystal Ordering Enhances Thermal Transport and Mechanics in Single-Domain Colloidal Nanocrystal Superlattices. *Nano Lett.* **2022**, *22*, 4669−4676.
(32) Kovalenko, M. V.; Scheele, M.; Talapin, D. V. Colloidal Nanocrystals with Molecular Metal Chalcogenide Surface Ligands. *Science* **2009**, *324*, 1417−1420.
(33) Scalise, E.; Srivastava, V.; Janke, E.; Talapin, D.; Galli, G.; Wippermann, S. Surface Chemistry and Buried Interfaces in All-Inorganic Nanocrystalline Solids. *Nat. Nanotechnol.* **2018**, *13*, 841−848.
(34) Fritzinger, B.; Capek, R. K.; Lambert, K.; Martins, J. C.; Hens, Z. Utilizing Self-Exchange to Address the Binding of Carboxylic Acid Ligands to CdSe Quantum Dots. *J. Am. Chem. Soc.* **2010**, *132*, 10195−10201.
(35) Newton, J. C.; Ramasamy, K.; Mandal, M.; Joshi, G. K.; Kumbhar, A.; Sardar, R. Low-Temperature Synthesis of Magic-Sized CdSe Nanoclusters: Influence of Ligands on Nanocluster Growth and Photophysical Properties. *J. Phys. Chem. C* **2012**, *116*, 4380−4389.
(36) Zhu, T. T.; Zhang, B. W.; Zhang, J.; Lu, J.; Fan, H. S.; Rowell, N.; Ripmeester, J. A.; Han, S.; Yu, K. Two-Step Nucleation of CdS Magic-Size Nanocluster MSC-311. *Chem. Mater.* **2017**, *29*, 5727−5735.
(37) Badia, A.; Singh, S.; Demers, L.; Cuccia, L.; Brown, G. R.; Lennox, R. B. Self-Assembled Monolayers on Gold Nanoparticles. *Chem. - Eur. J.* **1996**, *2*, 359−363.
(38) Badia, A.; Demers, L.; Dickinson, L.; Morin, F.; Lennox, R.; Reven, L. Gold − Sulfur Interactions in Alkylthiol Self-Assembled Monolayers Formed on Gold Nanoparticles Studied by Solid-State NMR. *J. Am. Chem. Soc.* **1997**, *119*, 11104−11105.
(39) Yu, W. W.; Qu, L. H.; Guo, W. Z.; Peng, X. G. Experimental Determination of the Extinction Coefficient of CdTe, CdSe, and CdS Nanocrystals. *Chem. Mater.* **2003**, *15*, 2854−2860.
(40) He, J.; Kanjanaboos, P.; Frazer, N. L.; Weis, A.; Lin, X. M.; Jaeger, H. M. Fabrication and Mechanical Properties of Large-Scale Freestanding Nanoparticle Membranes. *Small* **2010**, *6*, 1449−1456.
(41) Shi, X.; et al. Investigation of Mechanical Properties of Bedded Shale by Nanoindentation Tests: A Case Study on Lower Silurian Longmaxi Formation of Youyang Area in Southeast Chongqing, China. *Pet. Explor. Dev.* **2019**, *46*, 163−172.
(42) Choi, J. J.; Bealing, C. R.; Bian, K.; Hughes, K. J.; Zhang, W.; Smilgies, D.-M.; Hennig, R. G.; Engstrom, J. R.; Hanrath, T. Controlling Nanocrystal Superlattice Symmetry and Shape-Anisotropic Interactions through Variable Ligand Surface Coverage. *J. Am. Chem. Soc.* **2011**, *133*, 3131−3138.
(43) Landman, U.; Luedtke, W. D. Small Is Different: Energetic, Structural, Thermal, and Mechanical Properties of Passivated Nanocluster Assemblies. *Faraday Discuss.* **2004**, *125*, 1−22.
(44) Marsh, D. M. Plastic Flow in Glass. *Proc. R Soc. Lon Ser-A* **1964**, *279*, 420−426.
(45) Lee, D.; Jia, S. G.; Banerjee, S.; Bevk, J.; Herman, I. P.; Kysar, J. W. Viscoplastic and Granular Behavior in Films of Colloidal Nanocrystals. *Phys. Rev. Lett.* **2007**, *98*, 026103.
(46) Tan, J.-J.; Cheng, Y.; Zhu, W.-J.; Gou, Q.-Q. Elastic and Thermodynamic Properties of CdSe from First-Principles Calculations. *Commun. Theor. Phys.* **2008**, *50*, 220.
(47) Shenoy, V. B.; Johari, P.; Qi, Y. Elastic Softening of Amorphous and Crystalline Li−Si Phases with Increasing Li Concentration: A First-Principles Study. *J. Power Sources* **2010**, *195*, 6825−6830.
(48) Gao, F. M.; He, J. L.; Wu, E. D.; Liu, S. M.; Yu, D. L.; Li, D. C.; Zhang, S. Y.; Tian, Y. J. Hardness of Covalent Crystals. *Phys. Rev. Lett.* **2003**, *91*, 015502.
(49) Dong, A. G.; Ye, X. C.; Chen, J.; Kang, Y. J.; Gordon, T.; Kikkawa, J. M.; Murray, C. B. A Generalized Ligand-Exchange Strategy Enabling Sequential Surface Functionalization of Colloidal Nanocrystals. *J. Am. Chem. Soc.* **2011**, *133*, 998−1006.
(50) Nag, A.; Kovalenko, M. V.; Lee, J. S.; Liu, W. Y.; Spokoyny, B.; Talapin, D. V. Metal-Free Inorganic Ligands for Colloidal Nanocrystals: S^{2-}, HS^{-}, Se^{2-}, HSe^{-}, Te^{2-}, HTe^{-}, TeS_3^{2-}, OH^{-}, and NH_2^{-} as Surface Ligands. *J. Am. Chem. Soc.* **2011**, *133*, 10612−10620.
(51) Zhang, H.; Dasbiswas, K.; Ludwig, N. B.; Han, G.; Lee, B.; Vaikuntanathan, S.; Talapin, D. V. Stable Colloids in Molten Inorganic Salts. *Nature* **2017**, *542*, 328−331.
(52) Fotovvati, B.; Namdari, N.; Dehghanghadikolaei, A. On Coating Techniques for Surface Protection: A Review. *J. Manuf. Mater. Process.* **2019**, *3*, 28.

https://doi.org/10.1021/acs.nanolett.3c00674
Nano Lett. 2023, 23, 4916−4922